



Coexistence of DOPG model membranes and β -aescin micelles: a combined scattering and NMR study

Friederike Gräbitz-Bräuer¹ · Carina Dargel^{1,2} · Ramsia Geisler^{1,3} · Pascal Fandrich¹ · Viktor Sabadasch¹ · Lionel Porcar⁴ · Andreas Mix⁵ · Thomas Hellweg¹

Received: 14 March 2023 / Revised: 11 August 2023 / Accepted: 31 August 2023 / Published online: 25 September 2023
© The Author(s) 2023

Abstract

The saponin β -aescin is well known for its self-aggregation above the critical micelle concentration (*cmc*) and its interaction with model membranes made of zwitterionic phospholipids including the formation of mixed bicelle systems. In this study, we investigate the interaction of β -aescin with small unilamellar vesicles (SUVs) made of the negatively charged lipid 1,2-dioleoyl-*sn*-glycero-3-phosphoglycerol (DOPG). The study is conducted at a pH value at which aescin is negatively charged as well, and mixtures up to an aescin content of 50 mol% (equivalent to a molecular ratio of 1:1) were investigated, so that the *cmc* of aescin is exceeded by far. Analysis of the system by scattering and NMR methods was performed with respect to two reference systems made of the bare components: DOPG SUVs and aescin micelles. Wide-angle X-ray scattering (WAXS) was used to determine molecular correlation distances for both kinds of molecules, and small-angle neutron and X-ray scattering (SANS and SAXS) revealed a structural picture of the system, which was further confirmed by diffusion-ordered nuclear magnetic resonance spectroscopy (DOSY-NMR). Contrary to the expected solubilization of the DOPG membrane, most probably none- or only weakly-interacting, separated DOPG SUVs and aescin micelles were found. The study additionally highlights the importance of using independent methods to characterize a rather complex colloidal system in order to obtain a complete picture of the structures formed.

Keywords Small angle X-ray scattering (SAXS) · Small angle neutron scattering (SANS) · Wide angle X-ray scattering (WAXS) · Small unilamellar vesicles (SUV) · Micelles · 1,2-dioleoyl-*sn*-glycero-3-phosphoglycerol (DOPG) · Aescin · Saponin · Bio-surfactant · GIFT · SasView · Diffusion ordered spectroscopy (DOSY)

Friederike Gräbitz-Bräuer and Carina Dargel have contributed equally to this work.

✉ Thomas Hellweg
thomas.hellweg@uni-bielefeld.de

Friederike Gräbitz-Bräuer
friederike.graebitz@uni-bielefeld.de

Carina Dargel
cdargel@uni-muenster.de

Ramsia Geisler
Geisler@med.uni-frankfurt.de

Pascal Fandrich
p.fandrich@uni-bielefeld.de

Viktor Sabadasch
viktor.sabadasch@uni-bielefeld.de

Lionel Porcar
porcar@ill.eu

Andreas Mix
a.mix@uni-bielefeld.de

¹ Physical and Biophysical Chemistry, Bielefeld University, Universitätstraße 25, Bielefeld 33615, Germany

² Institute of Physical Chemistry, University of Münster, Corrensstraße 28/30, Münster 48149, Germany

³ Department II of Internal Medicine, Hematology/Oncology, Goethe University, Theodor-Stern-Kai 7, Frankfurt am Main 60590, Germany

⁴ Institute Laue-Langevin, 71 Avenue des Martyrs, Grenoble 38042, CEDEX 9, France

⁵ Lehrstuhl für Anorganische Chemie und Strukturchemie (ACS) and Centre for Molecular Materials (CM2), Bielefeld University, Universitätstraße 25, Bielefeld 33615, Germany

Introduction

Saponins are a vast group of plant-based biosurfactants, which usually have significant pharmacological activity [1–7]. Some of them are known to strongly interact with cell membranes and show haemolytic effects [1, 2, 8–10]. The saponin β -aescin from the horse chestnut tree (*Aesculus hippocastanum* L.; *Hippocastanaceae*), which is used in the present study, is known for its anti-edematous activity and shows also some anti-viral and anti-cancer activity [11–16]. Dargel et al. determined a critical micelle concentration (*cmc*) for β -aescin in phosphate buffer at pH=7.4 and 30 °C to be $cmc_{\text{aescin}} = (0.37 \pm 0.11)$ mM [17].

In previous studies, the interaction of β -aescin with vesicles based on the synthetic, zwitterionic lipid DMPC (1,2-dimyristoyl-*sn*-glycero-3-phosphocholine) has been studied [18–22]. In these works, the major finding was that such vesicles made of a saturated synthetic lipid show extremely strong interaction with β -aescin [18–20] and are completely decomposed to lipid nanodisks (bicelles) [21, 22].

Moreover, the interaction was found to partly depend on the DMPC phase state. It is found that low amounts of β -aescin change the bilayer mechanics, and in the L_α state, the bilayer shows an increased bending elastic constant. However, below the DMPC main phase transition temperature ($T_m = 24.5$ °C [23, 24]), the membrane appears to be softened by the saponin. The aim of the present work is to study the interaction of β -aescin with the lipid DOPG (1,2-dioleoyl-*sn*-glycero-3-phosphatidyl-glycerol). Phosphatidylglycerols (PG) are major components in plant leaves and are also found in many algae and bacterial species [25]. Moreover, PGs are also present in mammalian cells [26, 27].

DOPG is unsaturated and always in the fluid state above 0 °C due to $T_m = -18$ °C [27, 28]. In addition, its head

group is negatively charged. Hence, a different interaction with β -aescin compared to DMPC can be expected.

In the article at hand, we therefore address this question and study DOPG vesicles as model systems for bio-membranes in the presence of different amounts of β -aescin. The structures of DOPG and β -aescin are depicted in Fig. 1.

The interaction between the lipid and the saponin is scrutinized by combining NMR techniques and small/wide angle X-ray scattering (SAXS/WAXS). Moreover, to generate a different scattering contrast also small angle neutron scattering (SANS) is exploited. The covered mole fraction of β -aescin with respect to DOPG is $X_{\text{aescin}} = 0$ mol% up to $X_{\text{aescin}} = 50$ mol%.

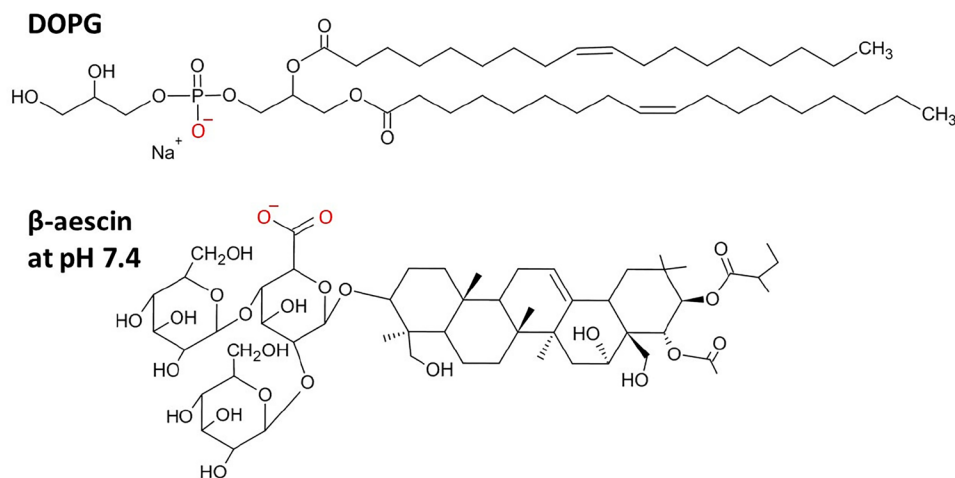
The major finding of this work is that DOPG vesicles are not decomposed into bicelles even at a mole fraction of $X_{\text{aescin}} = 50$ mol%. This was unexpected and is in contrast to previous results for saturated lipids and also in contrast to the observed haemolytic effect of aescin. Even low amounts of β -aescin are not interacting in a significant way with the DOPG membrane. On the contrary, β -aescin forms micelles for $X_{\text{aescin}} \geq cmc_{\text{aescin}}$, which coexist with the vesicles.

Materials and methods

Chemicals and sample preparation

The phospholipid 1,2-dioleoyl-*sn*-glycero-3-phosphoglycerol (DOPG) was purchased from Lipoid GmbH (Ludwigshafen, Germany, $\geq 99\%$ purity). The saponin β -aescin ($\geq 95\%$ purity, CAS-number 6805-41-0), chloroform, and deuteriumoxide (D_2O) were obtained from Sigma-Aldrich (Munich, Germany). All samples were prepared in a 50 mM phosphate buffer with pH/pD value of 7.4 in D_2O . All samples were produced with a lipid mass concentration of 15 mg/mL (equal to a molar concentration of 18.8 mM). The β -aescin content X_{aescin} varied between 0 and 50 mol%, whereby X_{aescin} relates

Fig. 1 Molecular structure of (top) the charged phospholipid 1,2-dioleoyl-*sn*-glycero-3-phosphoglycerol (DOPG) and (bottom) the saponin β -aescin at pH value of 7.4. The oxygen atoms of the deprotonated acidic group of β -aescin are highlighted in red



the amount of both substances, DOPG and aescin, and X_{aescin} is the mole fraction of the mixture:

$$X_{\text{aescin}} = \frac{n_{\text{aescin}}}{n_{\text{DOPG}} + n_{\text{aescin}}} \quad (1)$$

For the preparation of DOPG vesicles with different X_{aescin} , DOPG was dissolved in chloroform at first. The chloroform was removed using a rotary evaporator leading to the deposition of a thin DOPG film on the inner surface of the flask used. These films were stored over night at 60 °C. After drying, the lipid film was rehydrated with an aescin-containing buffer solution at the desired aescin concentration. After rehydration, all samples were subjected to five consecutive freeze-thaw cycles (in liquid nitrogen and warm water). To generate SUVs of a defined size, all samples were subsequently extruded (at least 15 passes, with increasing X_{aescin}) through the same membrane with a pore size of 50 nm (Whatman, Avanti Polar Lipids Inc., Alabama, USA) using a conventional extruder (extruder from Avanti Polar Lipids Inc., Alabama, USA).

A table which relates the aescin mole fraction X_{aescin} to the molar concentration of aescin can be found in the supporting information in Table S1. In the further text, the X_{aescin} with aescin concentrations above the cmc_{aescin} are written in italics and bold. In comparison to the DOPG-aescin-system, additionally pure aescin samples in the same phosphate buffer were prepared by dilution of a 18.8 mM stock solution. Only samples with aescin concentrations above the cmc were considered.

Small angle scattering (SAS)

The structure of colloidal particles like vesicular systems can be resolved by SAS experiments [29–32]. The magnitude of the scattering vector q (Eq. 2) depends on the scattered radiation detected at a scattering angle of 2θ . By using different kinds of radiation, thus different wavelengths λ , a broad q -range becomes accessible (Eq. 2).

$$q = \frac{4\pi}{\lambda} \cdot \sin(\theta) \quad (2)$$

The total scattering intensity $I(q)$ is given by Eq. 3.

$$I(q) = N \cdot (\Delta SLD)^2 \cdot V^2 \cdot P(q) \cdot S(q) \quad (3)$$

$I(q)$ depends on the number of particles N in a scattering volume V , the form factor $P(q)$, and structure factor $S(q)$. The scattering length density difference (ΔSLD) differs for SAXS and SANS and also depends on the solvent used. For X-ray scattering, the lipid head groups are highlighted because of their rather high electron density. In contrast, neutrons are scattered by the nuclei, and especially the proton rich part of the membrane becomes visible in SANS. The scattering

length densities for DOPG and β -aescin are presented in Table S3. A combination of both methods provides a more detailed picture of the membrane.

The overall shape of the mixed vesicles is obtained from the pair distance distribution function $p(r)$ in real space, which is obtained from standard indirect Fourier transform (IFT) implemented in the GIFT program from SAS data [33]. This method is shape independent and works without assuming a shape of the aggregates [34, 35]. The limitation for this calculation with GIFT is $D_{\text{max}} \leq \frac{\pi}{q}$.

Additional information on structural parameters of the SUVs are derived from model-dependent fitting with the *core multi shell (CMS)* model implemented in the program SasView [36–40]. SUV parameters such as the core radius R_C , its corresponding polydispersity σ_{R_C} , the membrane thickness d_z , and its corresponding polydispersity σ_{d_z} are derived. By using three shells ($n = 3$, n : number of shells) in the model, the membrane thickness can be divided into the thickness of the hydrophilic parts, or heads (shells number 1 and 3, d_{head}) and the thickness of the hydrophobic part, or tail (shell number 2, d_{tail}). The membrane thickness d_z can be calculated by Eq. 4.

$$d_z = 2 \cdot d_{\text{head}} + d_{\text{tail}} \quad (4)$$

Information about excess aescin micelles can be obtained from the *ellipsoid* model in SasView [36–38]. The polar radius (R_p) and the equatorial radius (R_e) of ellipsoids can be determined by fitting.

A customized model in SasView was implemented by Eq. 5 to determine the previously mentioned parameters for the SUV (model: *CMS* $n = 3$) and additionally parameters for an ellipsoid. The *CMS + ellipsoid* model is a sum of the *CMS* and *ellipsoid* models, which include the scale parameters S and the fit functions F themselves. B is an additional background.

$$CMS + ellipsoid \equiv (S_{\text{CMS}} \cdot F_{\text{CMS}} + S_{\text{ellipsoid}} \cdot F_{\text{ellipsoid}}) + B \quad (5)$$

Small angle neutron scattering (SANS)

SANS experiments were performed with samples prepared in D₂O buffer. Measurements were performed at the Institute Laue-Langevin (ILL) in Grenoble, France, using the D22 and D11 instruments. All samples in the range of $X_{\text{aescin}} = 0$ to 40 mol% were measured at the D22 instrument. The sample containing 50 mol% aescin was measured separately on the D11 instrument. For the D22 instrument, the samples were filled into 2 mm quartz cuvettes (Hellma Analytics, Müllheim, Germany) and measured at $T = 30$ °C in a 15-position sample holder. At a neutron wavelength of 6 Å with a sample to detector distance of 2.8 m and 17.6 m, and 12 Å at 17.6 m a q -range from $1.7 \cdot 10^{-3} \text{ \AA}^{-1}$ to 0.4 \AA^{-1} was

covered. The wavelength resolution was $\Delta \lambda/\lambda = 10\%$. For the D11 instrument, the sample was also filled into 2 mm quartz cuvettes (Hellma Analytics, Müllheim, Germany) and also measured at 30 °C in a similar 15-position sample holder. At a neutron wavelength of 6 Å with a sample to detector distance of 1.4 m, 8.0 m and 38.9 m a q -range from $1.6 \cdot 10^{-3} \text{ \AA}^{-1}$ to 0.4 \AA^{-1} was covered. The wavelength resolution was $\Delta \lambda/\lambda = 10\%$. With the software GRASP [41], provided by the ILL, the initial treatment of the 2D data was carried out. The final data was normalized with respect to the empty cell, background, and transmission from direct beam measurements.

Small angle X-ray scattering (SAXS)

SAXS experiments were performed on samples prepared in D₂O buffer on an inhouse SAXS/WAXS system (XEUSS, Xenocs, Sassenage, France) equipped with a CuK_α source ($\lambda = 1.541 \text{ \AA}$, GeniX Ultra low divergence, Xenocs) and a Pilatus 300K hybrid pixel detector (Dectris, Baden Deatwil, Switzerland). To cover a q -range from $6 \cdot 10^{-3}$ to 0.4 \AA^{-1} sample-to-detector distances of 0.8 m and 2.7 m were used for vesicle samples. For aescin micelle samples, a q -range from 0.05 to 0.3 \AA^{-1} was covered by a sample-to-detector distance of 0.8 m. Because of the small radii of the aescin micelles, it is sufficient to examine the aescin micelle samples only with SAXS at the mentioned distance. All samples were measured in a flow-through Kapton capillary (1 mm, GoodFellow GmbH, Bad Nauheim, Germany) positioned in a Linkam stage (Linkam Scientific, Tadworth, UK) at a temperature of 30 °C. The 2D data were analyzed using the Foxtrot software (V.3.3.4) [42] and normalized with respect to incident intensity, sample thickness, acquisition time, transmission, and background. By using glassy carbon type 2 as standard, the data were brought to absolute scale [43]. The normalized data were treated by the dynamic rebinned formalism implemented in the program SAXSutilities to improve statistics at high q -values (min. steps: 1, Δq : 0.005 \AA^{-1}) [44].

Wide angle X-ray scattering (WAXS)

WAXS-measurements were performed for samples prepared in D₂O buffer on the inhouse SAXS/WAXS system described in the “Small angle X-ray scattering (SAXS)” section. Experimental details and the data reduction procedure can be found in the same section. All measurements were performed at a temperature of 30 °C and a sample-to-detector distance of 0.16 m to cover a q -range from 0.5 \AA^{-1} to 2 \AA^{-1} . The peak observed in WAXS occurring at the position q_{WAXS} is directly related to the lateral molecule correlation distance d_{WAXS} via Eq. 6.

$$d_{\text{WAXS}} = \frac{2\pi}{q_{\text{WAXS}}} \quad (6)$$

Nuclear magnetic resonance spectroscopy (NMR)

Two dimensional NMR experiments like diffusion ordered NMR (DOSY-NMR) are excellently suited for determining the diffusion coefficient of molecules or structures in solution, like vesicles or micelles [45]. Thus, they can also provide insights into aggregation or incorporation processes in the liquid phase [46–48]. Species incorporated in the same aggregate exhibit the same diffusion coefficient. With the Stokes-Einstein equation (Eq. 7), the hydrodynamic radius R_H can be determined from D with the dynamic viscosity of the solvent η , the temperature T , and the Boltzmann-constant k_B .

$$D = \frac{k_B T}{6\pi\eta R_H} \quad (7)$$

The kinetic viscosity ν of the used phosphate buffer was determined at 30 °C using an Ubbelohde viscosimeter with a capillary constant of $k = 0.03088 \text{ m}^2\text{s}^{-2}$ (Schott Geräte, Mainz, Germany). The density of the phosphate buffer ρ was measured with a DMA 4500 density meter from Anton Paar (Graz, Austria). η was calculated from ν and ρ ($\eta = \nu \cdot \rho$) and determined to $\eta_{\text{buffer},30 \text{ °C}} = (1.04 \pm 0.01) \text{ mPa}\cdot\text{s}$.

Here, NMR experiments were performed on a BRUKER Avance NEO 600 FT NMR spectrometer (Bruker, Billerica, MA, USA), operating at a ¹H resonance frequency of 600.13 MHz. The instrument was equipped with a 5 mm CryoProbe Prodigy exhibiting a z -gradient coil delivering a maximum gradient strength of 6.57 G mm^{-1} at 10 Å. ¹H-NMR spectra were referenced to the residual protons of the deuterated solvents. The temperature unit of the instrument was calibrated according to the manual of the manufacturer of the instrument.

Diffusion NMR experiments have been performed using the *ledbpgp2s* pulse sequence delivered by the manufacturer. Proton diffusion data have been collected with 16k data points and a spectral width of 6000 Hz. The relaxation delay was set to 5 s.

The diffusion delay time (big Delta, Δ) was set to 100 ms. The gradient duration time (little delta, $\delta/2$) has been adjusted to values between 2300 and 3000 μs . The gradient strength within the diffusion experiments was incremented linearly using 16 steps. The diffusion data have been analyzed with the T1/T2 module of the BRUKER TopSpin® software package. The standard deviation of the experimentally determined gradient strength dependent signal intensities to the fitted decay function was $\leq 3.9 \cdot 10^{-2}$.

$^1\text{H-NMR}$ and $^1\text{H-DOSY}$ experiments were performed on samples containing pure DOPG vesicles, DOPG vesicles with $X_{\text{aescin}} = 1$ and **50** mol%, and samples containing aescin micelles with $c_{\text{aescin}} = 18.8$ mM, which is equivalent to $X_{\text{aescin}} = 50$ mol%.

Results

In this work, the influence of aescin on DOPG model membranes is studied with respect to aescin content X_{aescin} . All DOPG-aescin mixtures with X_{aescin} between 0 and 50 mol% were extruded and exhibit a bluish color typical for vesicle samples (see Fig. S1). No precipitation can be observed, even after several months, which means that formation of larger aggregates within the mixture can most probably be excluded independent on X_{aescin} .

The visual inspection already indicates that the interaction of DOPG and aescin shows clear differences compared to the well-studied DMPC-aescin system, in which the DMPC membrane gets solubilized into small bicelle particles by aescin at concentrations above cmc of aescin [21, 22]. For the present system, increasing the aescin concentration above the cmc -border (which corresponds to 2 mol% aescin) seems to have none or only a very minor effect. This is unexpected on the basis of the results for DMPC model membranes. Thus, the aim of the experiments described in the following is to clarify the picture of interaction between the DOPG model membranes and the aescin as added surfactant. Several scattering techniques (WAXS, SANS, and SAXS) and DOSY-NMR are exploited to follow this aim.

Lateral molecule correlation distance by WAXS (d_{WAXS})

WAXS-measurements are used to explore molecule-molecule distances in the particles present in the DOPG-aescin mixtures. Because of the large scattering angles, correlation signals of molecules located in nearest proximity can be resolved. By that, e.g., the distance between lipid (and additive) molecules in a lipid membrane or surfactant molecules in micelles can be determined. From the position of the WAXS-signal q_{WAXS} , the correlation distance d_{WAXS} (some authors call it headgroup distance when talking about lipid membranes) can be obtained by Eq. 6.

WAXS signals for mixtures composed of a fixed proportion of DOPG and varying amounts of aescin up to 50 mol% are presented in Fig. 2. The sample containing only the fixed amount of DOPG in the absence of aescin serves as a reference system (0 mol% aescin). For this system, a broad WAXS signal is obtained, which is in line with a lipid membrane adopting a liquid-crystalline L_{α} -phase [49]. The

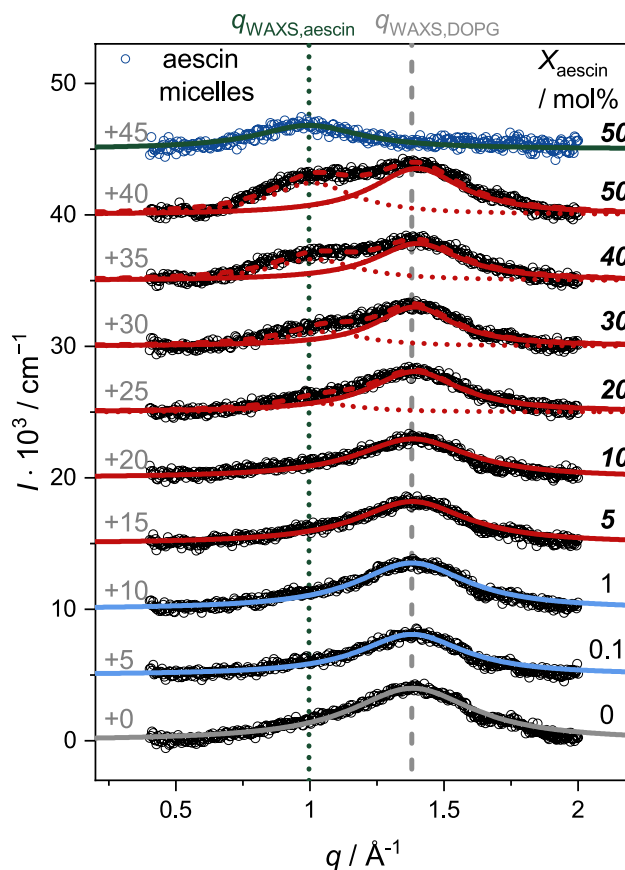


Fig. 2 WAXS signals of DOPG and aescin mixtures (black dots) and aescin micelles with a concentration equivalent to $X_{\text{aescin}} = 50$ mol% (blue dots). The aescin content X_{aescin} is represented by black numbers on the right. $X_{\text{aescin}} \geq cmc_{\text{aescin}}$ are presented by bold, italic numbers. For better readability, the data is shifted by the grey numbers on the left. Lorentzian fits are presented with solid lines for $d_{\text{WAXS,DOPG}}$, dotted lines for $d_{\text{WAXS,aescin}}$, and dashed lines for the sum of the individual functions. The vertical dashed and dotted line describe the positions of $q_{\text{WAXS,DOPG}}$ and $q_{\text{WAXS,aescin}}$

position of the maximum of the signal q_{WAXS} , determined by a Lorentzian fit, is given in Table S2 in the supplementary information, and d_{WAXS} calculated thereof with a value of ≈ 4.5 Å nicely corresponds to previous studies [49, 50].

Looking at the DMPC-aescin system, a contribution of aescin molecules to the WAXS signal of the mixture starting from any aescin content is also expected for the present system. Up to $X_{\text{aescin}} \leq 10$ mol%, only one Lorentzian fit is necessary to describe the scattering data. But, from an aescin content of 20 mol%, see Fig. 2, a second signal at lower q -value, corresponding to larger distances in real space and correlating with the larger volume of the aescin molecule compared to the DOPG (compare Fig. 1), arises. Hence, signals with $X_{\text{aescin}} \geq 20$ mol% are fitted by a sum of two Lorentzian functions representing the whole signals and providing two separate q_{WAXS} -values. These values are also

listed in Table S2, and the corresponding $d_{\text{WAXS,DOPG}}$ are presented in Table 1.

Compared to the DOPG-SUV-reference system, the position of the peak assigned to the DOPG molecules remains unchanged, so that $d_{\text{WAXS,DOPG}}$ does not change in dependence on X_{aescin} . This already indicates that the arrangement of most of the DOPG molecules stays unaffected by the addition of aescin molecules, even above the *cmc*, which is crossed at 2 mol% aescin. The correlation distance obtained from the position of the second signal does also not change as a function of X_{aescin} ; it remains approximately constant at 6.1 Å. Since only the aescin content is increased and the integral share I of the second Lorentzian function as well increases (see Table 1), the second contribution can most likely be assigned to structurally correlated aescin molecules. But it remains unknown whether the aescin molecules are integrated into the DOPG membrane of the SUV particles with a size of at most a few hundred nanometers or they are floating around as separate particles, e.g., micelles. From comparison with the DMPC-aescin system, the first option, incorporation into the DOPG membrane, is favored, as there, the appearance of the second WAXS signal can clearly be attributed to the incorporation of aescin into the lipid membrane [51]. But if this would also be the case for the present DOPG-aescin system, the incorporation into the DOPG membrane would most probably not lead to a solubilization of the lipid membrane, as indicated by the visual inspection of the samples.

To prove if the correlation distance of aescin molecules within an aescin micelle corresponds to the distance calculated from WAXS for the DOPG-aescin mixture, aescin micelles at a concentration equivalent to 50 mol% were prepared and investigated by WAXS. The signal obtained is also displayed in Fig. 2 and also yields a signal at $q_{\text{WAXS}} \approx 1 \text{ \AA}^{-1}$. Samples with lower aescin concentration starting from 20 mol% were additionally investigated (see Fig. S2), and all

obtained $d_{\text{WAXS,aescin}}$ values are listed in Table 1. Although the concentration of aescin corresponding to 20 mol% is already more than 5 times above the *cmc* determined by Dargel et al. [17], meaningful data was only obtained from this content on, due to the small signal intensity compared to the WAXS signal intensity of the solvent itself (similar molecule-molecule-distances in both the particles and the solvent). In comparison to the mixed system, the $d_{\text{WAXS,aescin}}$ values for the micelles are, including the errors, slightly larger, but nevertheless the assignment of this signal to origin from packed aescin molecules becomes obvious.

What cannot be stated from WAXS measurements is the location and the (possible) interaction of the DOPG and aescin molecules. To determine the kind(s) of structure(s) present in the mixed solution, small-angle scattering with X-rays and neutrons was performed next.

Pair distance distribution function $p(r)$ from IFT on SANS data

Due to the larger length scale resolved by small-angle scattering methods compared to the WAXS experiments discussed in the “Lateral molecule correlation distance by WAXS (d_{WAXS})” section, the shape of the particles present in the mixed DOPG-aescin solution can be determined thereof. First, only small-angle neutron scattering was used because of the good overall contrast between particles and solvent D_2O . For determination of the pair distance distribution function $p(r)$, which gives insights into the shape of the particles present, the indirect Fourier transformation (IFT) method was used applying the program GIFT [33].

The SANS data presented in Fig. 3 is very well suited for this analysis, because independent on X_{aescin} , a scattering plateau is reached at low q -values, indicating a well-defined particle size and allowing the whole particle dimension to be evaluated accurately. All curves measured show high similarity

Table 1 Lateral molecule correlation distances d_{WAXS} in DOPG-aescin mixtures with varying X_{aescin} and aescin micelles with concentrations equivalent to X_{aescin} obtained from Lorentzian fits to WAXS data (see Fig. 2). The relative integral I of each fit is given in %

X_{aescin} / mol%	Vesicle samples				Micelle samples	
	$d_{\text{WAXS,DOPG}}$ / Å	I / %	$d_{\text{WAXS,aescin}}$ / Å	I / %	$d_{\text{WAXS,aescin}}$ / Å	I / %
0	4.54 ± 0.05	(100)				
0.1	4.55 ± 0.05	(100)				
1	4.55 ± 0.05	(100)				
5	4.55 ± 0.05	(100)				
10	4.54 ± 0.05	(100)				
20	4.52 ± 0.05	(85)	6.07 ± 0.06	(15)	7.15 ± 0.18	(100)
30	4.52 ± 0.05	(73)	5.98 ± 0.06	(27)	6.73 ± 0.08	(100)
40	4.48 ± 0.05	(64)	6.21 ± 0.06	(35)	6.43 ± 0.07	(100)
50	4.49 ± 0.05	(61)	6.23 ± 0.06	(39)	6.31 ± 0.07	(100)

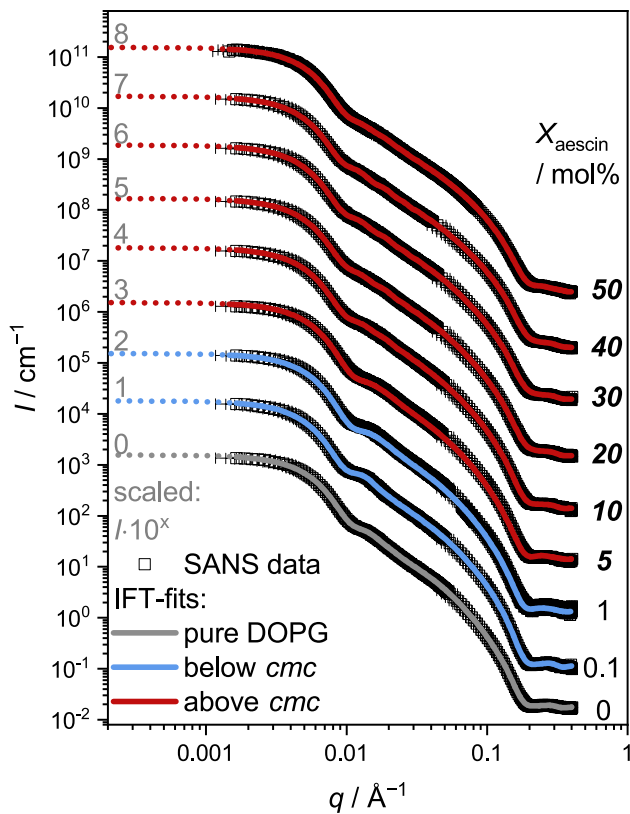


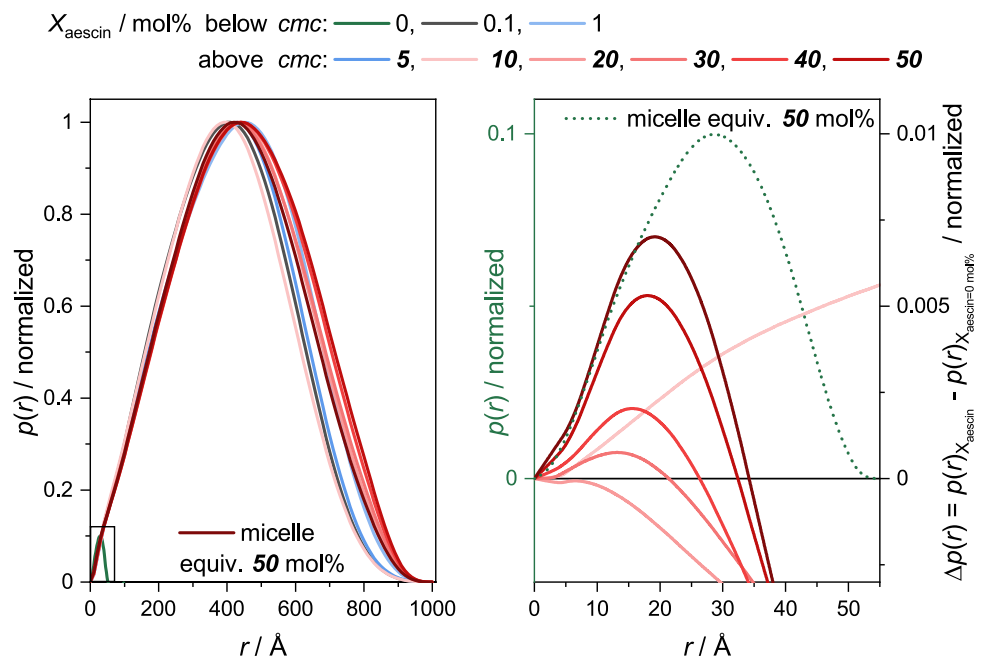
Fig. 3 SANS data with different X_{aescin} with IFT fits. X_{aescin} is indicated by black numbers on the right. The grey, blue, and red solid lines are an approximation resulting from IFT calculation with the program GIFT. For better readability, the curves are scaled by different multiples of 10, marked in grey numbers on the left. Dotted lines are extrapolations of the IFTs beyond the fit range at low q -values

to vesicle-like structures [19, 30, 50], and an influence of even an addition of 50 mol% aescin cannot be resolved by eye. To represent the formed structures in real space, the $p(r)$ -function was calculated for each X_{aescin} and displayed in Fig. 4a. The IFT fits to the scattering data are additionally shown in the same color coding as the $p(r)$ -function in Fig. 3. The shape of the $p(r)$ -functions nicely represents the presence of spherical particles, which might be polydisperse vesicles, for which normally such symmetric $p(r)$ -functions are obtained [52–54].

At high r , the $p(r)$ -functions all decay to zero, which on the one hand confirms the accurate determination of size and shape of the particles and on the other hand indicates that the size of the spherical particles seems to be unaffected by the addition of even 50 mol% aescin, which means a doubling of the total number of molecules present in the D_2O -solution. If all DOPG and aescin molecules are mixed to uniform particles, a size change in dependence on X_{aescin} would have been expected, and moreover $I(0)$, the scattering intensity of the plateau would also increase with increasing X_{aescin} , since $I(0)$ is proportional to the particle concentration. Neither is the case, which means that complete mixing of DOPG and aescin molecules seems unlikely.

Having a closer look at the low r -values of the $p(r)$ -function, a weak change in dependence on the increase of X_{aescin} becomes visible. The $p(r)$ -function of aescin micelles at a concentration equivalent to 50 mol% aescin obtained from SAXS measurements (see also Fig. 4 left for $p(r)$ -function and Fig. S3 for the fit to the data) indicates that the changes in the $p(r)$ -functions of the mixed system occur exactly in the size range of pure aescin micelles. To show this more clearly,

Fig. 4 Left: Normalized $p(r)$ functions calculated by IFT for SANS data of DOPG vesicles with X_{aescin} from 0 to 50 mol% (normalized to 1) and an aescin micelle with c_{aescin} equivalent to $X_{\text{aescin}} = 50$ mol% (normalized to 0.1). The black box indicates the zoomed area displayed in the right panel. The underlying data and fits for the $p(r)$ functions are shown in Fig. 3 and for the micelle in Fig. S4(a). Right: Zoom and comparison $\Delta p(r)$ for $X_{\text{aescin}} \geq \text{cmc}_{\text{aescin}}$ (right axis). In addition, the $p(r)$ function for aescin micelles with a concentration equivalent to $X_{\text{aescin}} = 50$ mol% is plotted in green for comparison (left axis)



again the pure DOPG sample is taken as reference, and the difference between the $p(r)$ -function at any $X_{\text{aescin}} > cmc$ to the pure DOPG as reference system is calculated. The resulting functions are depicted in Fig. 4 right and clearly show an increasing contribution to the $p(r)$ -function of the mixed system with increasing X_{aescin} . These results now give a clear indication for the coexistence of DOPG vesicles and aescin micelles and an increase of the number of micelles with increasing X_{aescin} . To further clarify if both kinds of particles are present without any interaction or are partially mixed, the complementary scattering method SAXS was used, which differs from SANS in a significantly changed contrast over the lipid membrane, whereof the incorporation of aescin molecules into the DOPG membrane shall be confirmed or excluded.

Model dependent fitting of SAXS and SANS data

In addition to the already presented SANS data, SAXS measurements were performed on exactly the same mixed DOPG-aescin samples. Both types of scattering data are shown in Fig. 5. Whereas for SANS, the resolution of the full particle size was possible, SAXS data does not show a plateau at low q due to the limited q -range of our setup. Moreover, the signal representing the particles in terms of size and polydispersity is much better resolved in SANS due to mainly two reasons: the better contrast of the liquid-crystalline membrane compared to the solvent and the much higher difference between scattering signal and background (flat for D_2O in SANS and strongly increased background with decreasing q in SAXS due to domination of

the background signal by the Kapton capillary). Hence, for such particles, our inhouse SAXS setup is not perfectly well suited to resolve the particle shape and size. But, in contrast to SANS, the lipid membrane contrast is not homogeneous in SAXS, and the chance of resolving an incorporation of aescin into the lipid membrane is high. The scattering data in Fig. 5b shows a strong change in dependence on the increase of X_{aescin} above the cmc of aescin. Below cmc , the homogeneous lipid membrane is clearly represented by the signal around 0.1 \AA^{-1} , and low polydispersity is indicated by the deep minimum at 0.04 \AA^{-1} .

An increase of X_{aescin} above the cmc leads to a vanishing of the minimum, which might indicate an increase in membrane polydispersity either by adhesion or (partial) incorporation of aescin molecules. At highest X_{aescin} , a conventional (lipid) membrane structure cannot be guessed any more, and the strong changes in the SAXS signal undoubtedly are attributed to the addition of aescin molecules.

Still, two possible scenarios are taken into consideration:

- I. Added aescin molecules are incorporated into the vesicular structures, and the change in the SAXS signal is attributed to this structural scenario.
- II. Added aescin molecules at concentrations above cmc assemble into micelles and coexist with DOPG vesicle.

For option I, as already mentioned, an increase in $I(0)$ is expected, which was not confirmed. Moreover, we tried to fit the SAXS data with a conventional three-shell sphere model representing a vesicle with inner-membrane contrast [50], but no good fits with reasonable parameters were obtained.

Fig. 5 Comparison of **a** SANS- and **b** SAXS data of DOPG vesicle samples with different X_{aescin} . The different X_{aescin} are given by the black number on the right. The scattering data is scaled by the grey numbers indicating multiples of 10 on the left. Also shown are the CMS-fits by red lines, and the CMS + ellipsoid-fits by blue lines

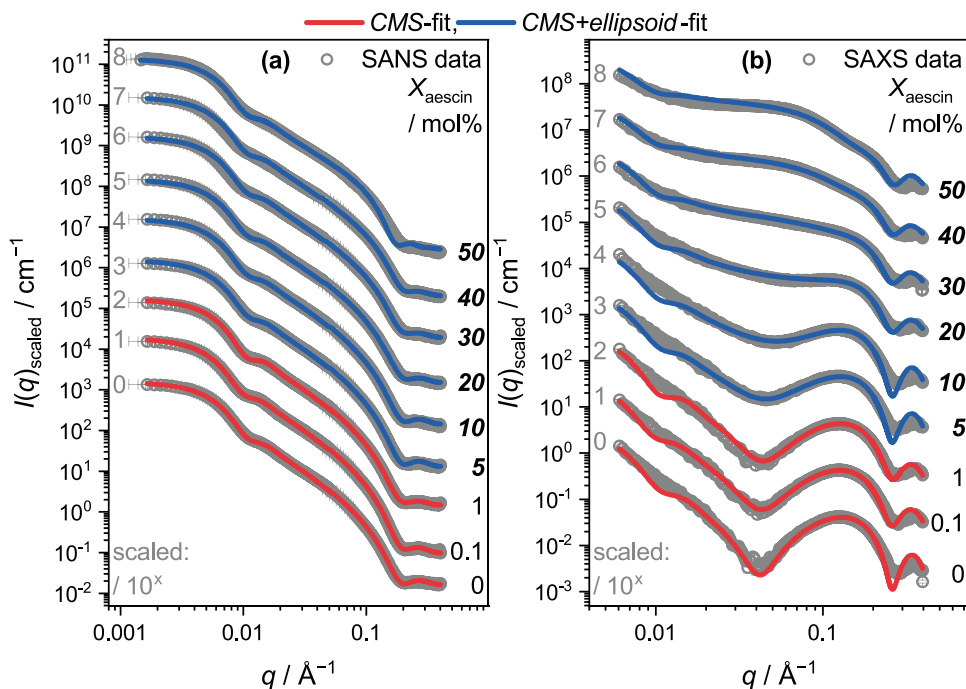


Table 2 Core radii R_C , radii polydispersities σ_{R_C} , and membrane thicknesses d_z obtained from *CMS* and *CMS + ellipsoid*-fitting to SANS and SAXS data. d_z was calculated from the fitted parameters for the tails (d_{tail} , see Table S6) and the fixed head thickness of $d_{\text{head}} = 4.1 \text{ \AA}$ [29]

X_{aescin} / mol%	$R_{C,\text{SANS}}$ / \AA	$\sigma_{R_{C,\text{SANS}}}$ / %	$d_{z,\text{SANS}}$ / \AA	$d_{z,\text{SAXS}}$ / \AA	Fitting model
0	205 ± 4	38	34.3 ± 0.7	38.9 ± 0.8	<i>CMS</i>
0.1	224 ± 4	38	34.4 ± 0.7	39.0 ± 0.8	<i>CMS</i>
1	224 ± 4	32	34.2 ± 0.7	38.7 ± 0.8	<i>CMS</i>
5	205 ± 4	38	34.5 ± 0.7	38.9 ± 0.8	<i>CMS + ellipsoid</i>
10	207 ± 4	38	34.4 ± 0.7	38.9 ± 0.8	<i>CMS + ellipsoid</i>
20	207 ± 4	38	34.1 ± 0.7	38.8 ± 0.8	<i>CMS + ellipsoid</i>
30	208 ± 5	39	34.3 ± 0.7	38.8 ± 0.8	<i>CMS + ellipsoid</i>
40	209 ± 4	39	34.2 ± 0.7	38.9 ± 0.8	<i>CMS + ellipsoid</i>
50	207 ± 4	39	34.4 ± 0.7	39.0 ± 0.8	<i>CMS + ellipsoid</i>

Therefore, we tried to prove option II. If DOPG vesicles and aescin micelle coexist without strong interactions, the scattering signal of the mixed sample should be representable by the sum of the scattering signals of the reference systems. To not only add the scattering intensities, but to moreover extract precise information about the particle size and contrast parameters, model fits for the reference systems are performed, afterwards summed up, compared to the data, and finally optimized to it.

As named above, pure DOPG vesicles and aescin micelles with X_{aescin} corresponding aescin concentrations were used as reference systems. To model the vesicular DOPG structures, the well-established *core multi shell (CMS)* model from the program SasView was used [36–40]. Using this model, the inner radius of the vesicles R_C and their polydispersity σ_{R_C} can be obtained. Furthermore, by using 3 shells, the thickness of the head groups d_{head} (shell 1 and 3) and the thickness of the hydrophobic parts of the membrane d_{tail} (shell 2) can be considered. Here, the thickness of the head group is fixed at $d_{\text{head}} = 4.1 \text{ \AA}$ [29]. The scattering length densities (*SLD*) used are presented in Table S3. For fitting the data, the protocol as described by Dargel et al. was

used [50]. The fits to the DOPG reference sample are displayed in Fig. 5, and the fit parameters are given in Tables 2 and S4 to S6. All fit parameters are in good agreement with the study on DOPG and the saponin glycyrrhizin, in which the same fit routine was used [50].

Modeling the data of the micelle reference system was done according to a study by Dargel et al. [17], in which aescin micelles in H_2O -solution also measured by SAXS were fitted. An ellipsoidal micelle shape was found which is why also in this study an ellipsoidal model from SASView was used for fitting [36–38]. This model yields ellipsoidal parameters, the equatorial radius R_e and the polar radius R_p . Furthermore, the scale and background can be adjusted. The *SLD* for aescin is presented in Table S3. The fits to the SAXS data are presented in Fig. S5, and the resulting parameters are shown in Tables 3 and S4. The ratio of $R_{p,\text{SAXS}}$ and $R_{e,\text{SAXS}}$ given in Table 3 shows that for smaller X_{aescin} , the micelles are elongated, and with increasing X_{aescin} , the micelles become more spherical. This trend was also described by Dargel et al. for aescin micelles in H_2O -buffer [17].

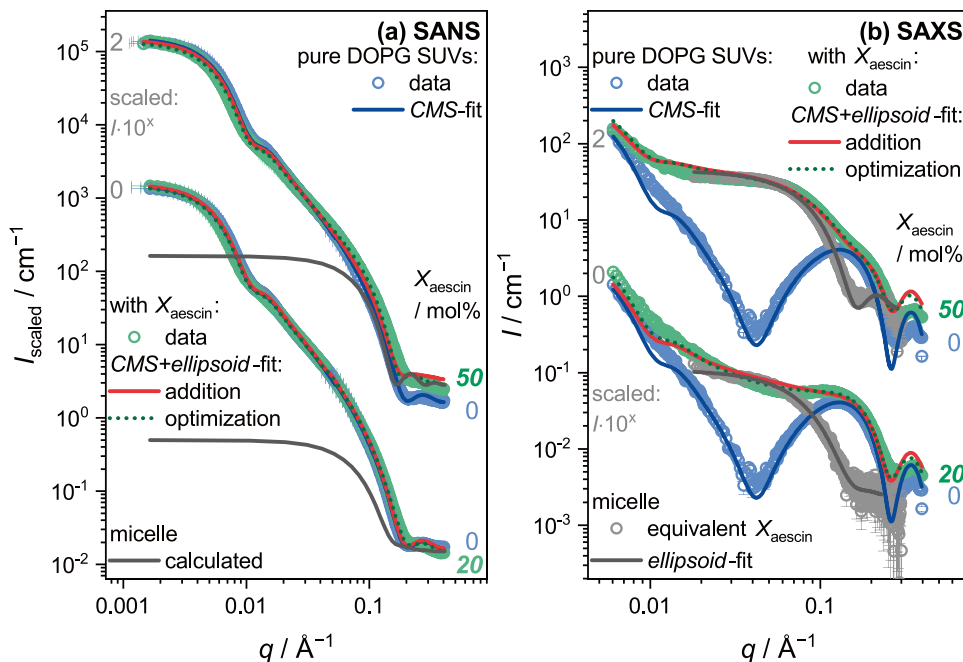
The scattering data of both model systems was now fitted, and the fit functions can be used to investigate hypothesis II. Both models are summed up to the customized *CMS+ellipsoid*-model, which combines the both individual models and adds an additional background (see Eq. 5). In simplified terms, each model consists of a fit function F , from which structure-relevant parameters can be extracted, and a scaling factor S . If both particle types are present independently of one another, it should not be necessary to change both F and S significantly after summation into the customized model in order to describe the scattering data of the mixed system adequately.

Figure 6 shows the fits to the reference systems as well as with the customized model for the mixed sample for two exemplary aescin contents of 20 mol% (the lowest concentration for which an effect of the aescin addition became visible by all methods used) and 50 mol% (the highest concentration investigated). Since aescin micelles were not measured by SANS, the fit function for the ellipsoidal micelle was determined from SAXS data and then converted

Table 3 Ellipsoid parameters from fitting with the *CMS + ellipsoid* and *ellipsoid* models in SasView for SANS and SAXS data of DOPG vesicle samples and for SAXS data of aescin micelle samples

X_{aescin} / mol%	DOPG SUVs + aescin				Aescin micelles	
	$R_{p,\text{SANS}}$ / \AA	$R_{e,\text{SANS}}$ / \AA	$R_{p,\text{SAXS}}$ / \AA	$R_{e,\text{SAXS}}$ / \AA	$R_{p,\text{SAXS}}$ / \AA	$R_{e,\text{SAXS}}$ / \AA
5	12.2 ± 0.3	57.6 ± 1.2	13.0 ± 0.3	36.6 ± 0.8	13.7 ± 0.2	40.3 ± 0.4
10	13.1 ± 0.3	54.2 ± 1.1	13.3 ± 0.3	39.1 ± 0.8	15.9 ± 0.2	39.4 ± 0.4
20	14.0 ± 0.3	39.6 ± 0.8	19.4 ± 0.4	32.0 ± 0.6	19.7 ± 0.2	32.1 ± 0.3
30	14.3 ± 0.3	27.5 ± 0.6	21.3 ± 0.4	30.1 ± 0.6	21.8 ± 0.3	30.3 ± 0.3
40	14.6 ± 0.3	25.5 ± 0.5	23.4 ± 0.5	28.9 ± 0.6	23.9 ± 0.3	29.0 ± 0.3
50	23.9 ± 0.5	27.7 ± 0.6	26.1 ± 0.5	26.8 ± 0.5	26.9 ± 0.3	26.9 ± 0.3

Fig. 6 Comparison of DOPG vesicles with $X_{\text{aescin}} = 0$ mol% (blue) to vesicles with 20 and 50 mol% (green), and micelle samples with equivalent X_{aescin} (grey). **a** SANS and **b** SAXS data; the different X_{aescin} are given by the green numbers on the right. The scattering data is scaled by the grey numbers indicating multiples of 10 on the left. Also shown are the CMS-fits for pure DOPG vesicles by blue lines. For aescin containing samples are shown the CMS + ellipsoid-fits by red lines for pure addition and by green dotted lines after optimization. For aescin micelles, the SAXS data and ellipsoid-fits are shown in grey in **b**; furthermore, with SasView, calculated SANS patterns are shown in **a** [37]



to a SANS curve using the known contrast parameters. Bare addition of the single model functions already led to a very good agreement between the CMS+ellipsoid-model and the experimental data of the mixed system. A final optimization of the fit parameters (scale and size variables) did not lead to a significant improvement of the fit quality (see Fig. 6).

The results obtained by this fitting strategy thus clearly prove that DOPG vesicles and aescin micelles coexist with each other in solution. From the comparison of the SANS and SAXS data of the mixed system, including the data for the reference systems, it becomes also clear why the influence of the increase in X_{aescin} in the case of SANS has no significant impact. Due to the small size of the aescin micelles, their contribution to the total scattering intensity is small. This becomes obvious, for example, at small q values in the case of SANS. The contribution of the scattering intensity of the aescin micelles is below 0.05 %. At high q values, e.g., in the range of the membrane signal ($q \approx 0.1 \text{ \AA}^{-1}$), the contribution for SANS is still at most 10%, here also because the lipid membrane itself shows a high scattering intensity. This is exactly not the case for SAXS, since due to multi-layered membrane contrast, interference effects lead to the formation of the previously described minimum-maximum structure of the scattering intensity. The scattering intensity of the aescin micelles is now added to this low-intensity pattern, which results in a high contribution of the aescin micelles concerning the total intensity. The scattering intensity in this q -range is increased significantly. This example impressively shows how important the complementary analysis of a system using different methods or different scattering contrasts can be and that the use of only one method can lead to a

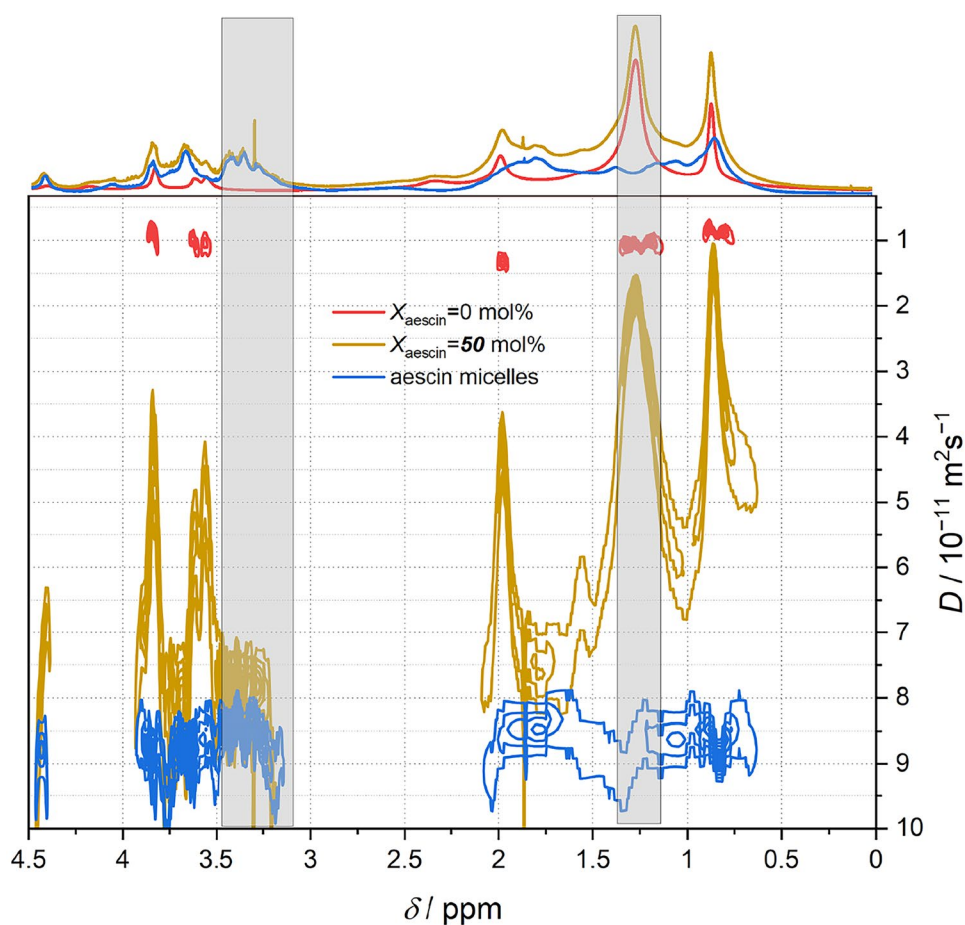
completely wrong understanding of the system if the structural conception of the system cannot be substantiated by other, independent methods.

Two questions have not yet been answered by the methods used so far: are significant interactions between the DOPG and the aescin molecules observable, i.e., do the DOPG vesicles and the aescin micelles interact partially adhesively and diffuse through the solution as agglomerates at least temporarily? And is a part of the aescin molecules incorporated into the DOPG vesicles, so that interactions at closest spatial distance would have to be detected? Both questions should finally be clarified by using NMR methods.

Spatial interaction and proximity of DOPG and aescin molecules by DOSY-NMR

The DOSY-NMR method was used to determine the diffusion coefficients D of the DOPG and aescin molecules in the mixed solutions. Again, the two reference samples, pure DOPG vesicles and aescin micelles, were used. Via the NMR signals of unique protons in both reference systems and the comparison to the mixed system, the spatial interaction between the DOPG vesicles and the aescin micelles can be proven within the sensitivity limits of the method. Only the highest aescin content of 50 mol% was used due to the comparably low sensitivity of the method. The recorded DOSY spectra for all three systems are shown in Fig. 7. On top of the DOSY signals, additionally, the ^1H NMR signals of the mentioned samples are given. The peak allocation to the ^1H -signals is presented in Figs. S6 and S7.

Fig. 7 ^1H DOSY plots of (red) pure DOPG vesicles, (blue) aescin micelles equivalent to $X_{\text{aescin}} = 50$ mol%, and (yellow) DOPG vesicles with $X_{\text{aescin}} = 50$ mol%. Highlighted are the signal at $\delta = 1.26$ ppm and the region between 3.1 ppm and 3.5 ppm



The one dimensional ^1H -spectra show a severe overlap of resonances of both components. However, the signal at a chemical shift of $\delta = 1.26$ ppm is mainly caused by $-\text{CH}_2$ groups located in the DOPG tails, while the multiplets between $\delta = 3.1$ ppm and 3.5 ppm can be assigned to the glucose parts of the aescin molecule [17]. These substance specific signals are now used for the determination of the diffusion coefficients D of the DOPG SUVs and the aescin micelles and further for the subsequent comparison with the mixed system. For the pure DOPG vesicles, the diffusion coefficient is given by $D_{\text{DOPG}} = (8.5 \pm 1.1) \cdot 10^{-12} \text{ m}^2 \text{ s}^{-1}$, and for the aescin micelles, D_{aescin} is found to be $(8.1 \pm 0.7) \cdot 10^{-11} \text{ m}^2 \text{ s}^{-1}$. The diffusion coefficients of both reference systems differ by one order of magnitude. Hence, DOPG vesicles and aescin micelles can be easily distinguished based on their D values. With the Stokes-Einstein equation (see Eq. 7), the hydrodynamic radii are determined to $R_{\text{H,DOPG}} = (241 \pm 26) \text{ \AA}$ and $R_{\text{H,aescin}} = (26 \pm 3) \text{ \AA}$. The values agree very well with the already determined values of d_z , R_c for pure DOPG vesicles (see Table 2) and R_c and R_p for aescin micelles with $X_{\text{aescin}} = 50$ mol% (see Table 3).

Especially the signals focused above are now compared to the DOSY spectrum of the mixed system containing 50 mol% aescin (Fig. 7, yellow). If mixed particles are present, the

substance specific signals must show contributions of both particles, vesicles and micelles. A change in D is visible for both signals; for both cases, D is shifted in the direction of the “opposite reference system,” but there is no overlap with this “opposite” particle type (e.g., with the D for DOPG vesicles for the aescin signal at $\delta = 3.1$ ppm and 3.5 ppm).

These results indicate that in the mixed system, almost all aescin molecules are located in micelles and almost no aescin is incorporated into the DOPG vesicles. However, the low sensitivity of the NMR method must be taken into account here, so that an incorporated fraction may be below the detection limit. The shift of D in the direction of the opposite particle type nevertheless indicates that a slight association of aescin molecules and micelles to DOPG vesicles might be possible.

Conclusion

Interactions of the lipid DOPG with the negatively charged head group and with the negatively charged saponin aescin were studied in this work in a D_2O -buffer solution at a pH value of 7.4. To correlate the species found in mixture with a ratio up to an aescin content X_{aescin} of 50 mol%

(equivalent to a ratio of 1:1), DOPG SUVs and aescin micelles at concentrations appropriate to X_{aescin} were investigated as well. In contrast to previous studies on DMPC vesicles, here no decomposition of the DOPG vesicles occurs at any aescin molar ratio.

An important concentration in this system is the *cmc* of aescin which is reached at contents higher than 2 mol%.

Different scattering and the NMR method DOSY are used to investigate the system. WAXS measurements showed the contributions of correlated molecules from both substances, DOPG and aescin. However, based on this method, it was impossible to clarify whether the correlation signal of the aescin molecules detectable well above the *cmc* arises from aescin molecules incorporated into the DOPG membrane or from independent aescin micelles. Small angle scattering with neutrons and X-ray clearly revealed the coexistence of both, DOPG SUVs and aescin micelles. Especially the model-dependent fitting clearly showed that the data of the mixed system can be represented by a sum of the signals of both reference systems. Optimization of the fit function did not lead to a significant improvement of the fit quality as well as a change in the fit parameters. This observation leads to the assumption that DOPG vesicles and aescin micelles do not, for instance, stick to each other or that lipid molecules and aescin partially mix. This is further proven by DOSY measurements which presented only a slight change in the diffusion coefficients of the single components in the mixed system compared to the reference systems, indicating only a very weak interaction and no incorporation of significant amount of aescin in the lipid bilayer.

Compared to the well-investigated DMPC-aescin system, a huge difference concerning the intermolecular interactions between both substances is observed here. We suggest that the avoidance of the mixing of both substances is mainly caused by the negative charges which are located in the hydrophilic parts of both substances. The lipid DMPC as well carries a negative charge in the hydrophilic head group, but while interacting with the negatively charged aescin, the charges might be compensated within the membrane by the positive charge also present in the DMPCs head group. Exactly this compensation within the membrane is missing in this system, which might lead to the observed repulsion of the molecules and formation of the separate, mostly independent structures. Investigations from the theoretical point of view would be very interesting here to clarify the reason for the very different behavior of both systems.

We want to especially point out the importance of verification of results by independent methods in such multi-component systems. Having a look at only the SANS data, a change of the system upon addition of aescin is only hardly detectable. One would assume that still, only DOPG SUVs

are present in the sample. But having a look at the SAXS results too, strong changes became obvious.

A coexistence of vesicles and micelles was described previously [55–57], but to our knowledge, it has never been described for a phospholipid/saponin system, like the one used in the present work.

Supplementary Information The online version contains supplementary material available at <https://doi.org/10.1007/s00396-023-05168-0>.

Acknowledgements The authors thank the ILL for granting the beamtime at the D22 and D11 beamlines that was available as part of proposal 9-11-1824 and 9-13-898 (doi:10.5291/ILL-DATA.9-11-1824 and 10.5291/ILL-DATA.9-13-898). Furthermore, the authors thank Ralf Schweins for his support during the beamtime at the D11. The authors thank Otto Glatter for providing the PCG software package, the fruitful discussion, and help with the software.

Author contributions F.G.-B. has prepared the samples, conducted the SAXS/WAXS experiments, and analyzed all recorded data. Additionally, F.G.-B. has written important parts of the manuscript. C.D. supported F.G.-B. in the evaluation of the whole data set and also wrote important parts of the manuscript. R.G. has participated in the SANS experiments at the ILL, contributed to the initial data reduction, and helped with coordinating the project; she has also edited the manuscript. P.F. and V.S. participated in the experiments at the ILL and contributed to writing the manuscript. L.P. was the local contact during the SANS beamtime at the ILL and helped with setting up the sample environment, with the initial data reduction, and has revised the manuscript. A.M. performed the NMR experiments, discussed the data analysis, and has written parts of the manuscript. T.H. coordinated the project, discussed the data analysis with F.G.-B. and C.D., and has written important parts of the manuscript. All authors reviewed the manuscript.

Funding Open Access funding enabled and organized by Projekt DEAL.

Data availability Data can be obtained from the authors upon request.

Declarations

Ethics approval and consent to participate Does not apply.

Consent for publication Not applicable.

Conflict of interest The authors declare no competing interests.

Open Access This article is licensed under a Creative Commons Attribution 4.0 International License, which permits use, sharing, adaptation, distribution and reproduction in any medium or format, as long as you give appropriate credit to the original author(s) and the source, provide a link to the Creative Commons licence, and indicate if changes were made. The images or other third party material in this article are included in the article's Creative Commons licence, unless indicated otherwise in a credit line to the material. If material is not included in the article's Creative Commons licence and your intended use is not permitted by statutory regulation or exceeds the permitted use, you will need to obtain permission directly from the copyright holder. To view a copy of this licence, visit <http://creativecommons.org/licenses/by/4.0/>.

References

- Lorent JH, Quetin-Leclercq J, Mingeot-Leclercq M-P (2014) The amphiphilic nature of saponins and their effects on artificial and biological membranes and potential consequences for red blood and cancer cells. *Org Biomol Chem* 12(44):8803–8822. <https://doi.org/10.1039/c4ob01652a>
- Güçlü-Ustündağ O, Mazza G (2007) Saponins: properties, applications and processing. *Crit Rev Food Sci Nutr* 47(3):231–258. <https://doi.org/10.1080/10408390600698197>
- Liu J, Henkel T (2002) Traditional Chinese Medicine (TCM): are polyphenols and saponins the key ingredients triggering biological activities? *Curr Med Chem* 9(15):1483–1485. <https://doi.org/10.2174/0929867023369709>
- Alice CB, Vargas VMF, Silva GAAB, de Siqueira NCS, Schapoval EES, Gleye J, Henriques JAP, Henriques AT (1991) Screening of plants used in South Brazilian folk medicine. *J Ethnopharmacol* 35(2):165–171. [https://doi.org/10.1016/0378-8741\(91\)90069-P](https://doi.org/10.1016/0378-8741(91)90069-P)
- Kerwin SM (2004) Soy saponins and the anticancer effects of soybeans and soy-based foods. *Curr Med Chem Anticancer Agents* 4(3):263–272. <https://doi.org/10.2174/1568011043352993>
- Vincken J-P, Heng L, de Groot A, Gruppen H (2007) Saponins, classification and occurrence in the plant kingdom. *Phytochemistry* 68(3):275–297. <https://doi.org/10.1016/j.phytochem.2006.10.008>
- Góral I, Wojciechowski K (2020) Surface activity and foaming properties of saponin-rich plants extracts. *Adv Coll Interface Sci* 279:102145. <https://doi.org/10.1016/j.cis.2020.102145>
- Gurfinkel DM, Rao AV (2003) Soyasaponins: the relationship between chemical structure and colon anticarcinogenic activity. *Nutr Cancer* 47(1):24–33. https://doi.org/10.1207/s15327914nc4701_3
- Kim S-W, Park S-K, Kang S-I, Kang H-C, Oh H-J, Bae C-Y, Bae D-H (2003) Hypocholesterolemic property of *Yucca schidigera* and *Quillaja saponaria* extracts in human body. *Arch Pharmacol Res* 26(12):1042–1046. <https://doi.org/10.1007/BF02994756>
- Cheeke PR (2000) Actual and potential applications of *Yucca schidigera* and *Quillaja saponaria* saponins in human and animal nutrition. In: Oleszek, W., Marston, A. (eds.) *Saponins in food, feedstuffs and medicinal plants*. Springer eBook Collection, pp. 241–254. Springer, Dordrecht. https://doi.org/10.1007/978-94-015-9339-7_5
- Sirtori CR (2001) Aescin: pharmacology, pharmacokinetics and therapeutic profile. *Pharmacol Res* 44(3):183–193. <https://doi.org/10.1006/phrs.2001.0847>
- Tsibranska S, Ivanova A, Tcholakova S, Denkov N (2021) Structure and undulations of escin adsorption layer at water surface studied by molecular dynamics. *Molecules* (Basel, Switzerland) 26(22). <https://doi.org/10.3390/molecules26226856>
- Khan T, Khan MA, Mashwani Z-U-R, Ullah N, Nadhman A (2021) Therapeutic potential of medicinal plants against COVID-19: the role of antiviral medicinal metabolites. *Biocatal Agric Biotechnol* 31:101890. <https://doi.org/10.1016/j.bcab.2020.101890>
- Sparg SG, Light ME, van Staden J (2004) Biological activities and distribution of plant saponins. *J Ethnopharmacol* 94(2–3):219–243. <https://doi.org/10.1016/j.jep.2004.05.016>
- Vasiliauskas A, Leonavičienė L, Vaitkienė D, Bradūnaitė R, Lukšienė A (2010) Anti-inflammatory effects of *Aesculus hippocastanum* L. tincture and the pro-/antioxidant bodily state of rats with adjuvant arthritis. *Acta Medica Lituanica* 17(3):123–132. <https://doi.org/10.2478/v10140-010-0016-6>
- Costantini A (1999) Escin in pharmaceutical oral dosage forms: quantitative densitometric HPTLC determination. *II Farmaco* 54(11–12):728–732. [https://doi.org/10.1016/S0014-827X\(99\)00090-7](https://doi.org/10.1016/S0014-827X(99)00090-7)
- Dargel C, Geisler R, Hannappel Y, Kemker I, Sewald N, Hellweg T (2019) Self-assembly of the bio-surfactant aescin in solution: a small-angle X-ray scattering and fluorescence study. *Colloids and Interfaces* 3(2):47. <https://doi.org/10.3390/colloids3020047>
- Sreij R, Dargel C, Moleiro LH, Monroy F, Hellweg T (2017) Aescin incorporation and nanodomain formation in DMPC model membranes. *Langmuir: The ACS Journal of Surfaces and Colloids* 33(43):12351–12361. <https://doi.org/10.1021/acs.langmuir.7b02933>
- Sreij R, Dargel C, Geisler P, Hertle Y, Radulescu A, Pasini S, Perez J, Moleiro LH, Hellweg T (2018) DMPC vesicle structure and dynamics in the presence of low amounts of the saponin aescin. *Phys Chem Chem Phys* 20(14):9070–9083. <https://doi.org/10.1039/c7cp08027a>
- Sreij R, Dargel C, Hannappel Y, Jestin J, Prévost S, Dattani R, Wrede O, Hellweg T (2019) Temperature dependent self-organization of DMPC membranes promoted by intermediate amounts of the saponin aescin. *BBA-Biomembranes* 1861(5):897–906. <https://doi.org/10.1016/j.bbamem.2019.01.015>
- Geisler R, Pedersen MC, Hannappel Y, Schweins R, Prévost S, Dattani R, Arleth L, Hellweg T (2019) Aescin-induced conversion of gel-phase lipid membranes into bicelle-like lipid nanoparticles. *Langmuir: The ACS Journal of Surfaces and Colloids*. <https://doi.org/10.1021/acs.langmuir.9b02077>
- Geisler R, Pedersen MC, Preisig N, Hannappel Y, Prévost S, Dattani R, Arleth L, Hellweg T (2021) Aescin - a natural soap for the formation of lipid nanodiscs with tunable size. *Soft Matter* 17(7):1888–1900. <https://doi.org/10.1039/D0SM02043E>
- Koynova R, Caffrey M (1998) Phases and phase transitions of the phosphatidylcholines. *Biochem Biophys Acta* 1376(1):91–145. [https://doi.org/10.1016/s0304-4157\(98\)00006-9](https://doi.org/10.1016/s0304-4157(98)00006-9)
- Du L, Liu X, Huang W, Wang E (2006) A study on the interaction between ibuprofen and bilayer lipid membrane. *Electrochim Acta* 51(26):5754–5760. <https://doi.org/10.1016/j.electacta.2006.03.009>
- Garidel P, Johann C, Mennicke L, Blume A (1997) The mixing behavior of pseudobinary phosphatidylcholine-phosphatidylglycerol mixtures as a function of pH and chain length. *Eur Biophys J* 26(6):447–459. <https://doi.org/10.1007/s002490050099>
- Himeno H, Shimokawa N, Komura S, Andelman D, Hamada T, Takagi M (2014) Charge-induced phase separation in lipid membranes. *Soft Matter* 10(40):7959–7967. <https://doi.org/10.1039/c4sm01089b>
- Findlay EJ, Barton PG (1978) Phase behavior of synthetic phosphatidylglycerols and binary mixtures with phosphatidylcholines in the presence and absence of calcium ions. *Biochemistry* 17(12):2400–2405. <https://doi.org/10.1021/bi00605a023>
- Brown KL, Conboy JC (2015) Phosphatidylglycerol flip-flop suppression due to headgroup charge repulsion. *J Phys Chem B* 119(32):10252–10260. <https://doi.org/10.1021/acs.jpcc.5b05523>
- Pan J, Heberle FA, Tristram-Nagle S, Szymanski M, Koepfinger M, Katsaras J, Kučerka N (2012) Molecular structures of fluid phase phosphatidylglycerol bilayers as determined by small angle neutron and X-ray scattering. *Biochem Biophys Acta* 1818(9):2135–2148. <https://doi.org/10.1016/j.bbamem.2012.05.007>
- Kučerka N, Nieh MP, Katsaras J (2010) Small-angle scattering from homogenous and heterogeneous lipid bilayers. vol. 12, pp. 201–235. <https://doi.org/10.1016/B978-0-12-381266-7.00008-0>
- Kiselev MA, Zemlyanaya EV, Aswal VK, Neubert RHH (2006) What can we learn about the lipid vesicle structure from the small-angle neutron scattering experiment? *Eur Biophys J* 35(6):477–493. <https://doi.org/10.1007/s00249-006-0055-9>
- Kiselev MA, Lombardo D (2017) Structural characterization in mixed lipid membrane systems by neutron and X-ray scattering. *Biochimica et Biophysica Acta General Subjects* 1861(1 Pt B), 3700–3717. <https://doi.org/10.1016/j.bbagen.2016.04.022>

33. Bergmann A, Fritz G, Glatter O (2000) Solving the generalized indirect Fourier transformation (GIFT) by Boltzmann simplex simulated annealing (BSSA). *J Appl Crystallogr* 33(5):1212–1216. <https://doi.org/10.1107/S002188980008372>
34. Glatter O (1977) A new method for the evaluation of small-angle scattering data. *J Appl Crystallogr* 10(5):415–421. <https://doi.org/10.1107/S0021889877013879>
35. Mittelbach R, Glatter O (1998) Direct structure analysis of small-angle scattering data from polydisperse colloidal particles. *J Appl Crystallogr* 31(4):600–608. <https://doi.org/10.1107/S0021889898002209>
36. Doucet M, Cho JH, Alina G, Bakker J, Bouwman W, Butler P, Campbell K, Gonzales M, Heenan R, Jackson A et al (eds.) (2019) *SasView* Version 4.2.2. Available Online: www.sasview.org/2019-05-20-release-4.2.2/
37. Doucet M, Cho JH, Alina G, Bakker J, Bouwman W, Butler P, Campbell K, Gonzales M, Heenan R, Jackson A et al (eds.) (2021) *SasView* Version 5.0.4. Version 5.0.4 was Released on Apr 07, 2021
38. Feigin LA, Svergun DI (1987) *Structure analysis by small-angle X-ray and neutron scattering*. Springer. <https://doi.org/10.1007/978-1-4757-6624-0>
39. Guinier A, Fournet G (1955) *Small angle scattering of X-rays* vol. 19. John Wiley & Sons, London. <https://doi.org/10.1002/pol.1956.120199326>
40. Kline SR (2006) Reduction and analysis of SANS and USANS data using IGOR Pro. *J Appl Crystallogr* 39(6):895–900. <https://doi.org/10.1107/S0021889806035059>
41. Rennie AR, Hellsing MS, Wood K, Gilbert EP, Porcar L, Schweins R, Dewhurst CD, Lindner P, Heenan RK, Rogers SE, Butler PD, Krzywon JR, Ghosh RE, Jackson AJ, Malfois M (2013) Learning about SANS instruments and data reduction from round robin measurements on samples of polystyrene latex. *J Appl Crystallogr* 46(5):1289–1297. <https://doi.org/10.1107/S0021889813019468>
42. Viguier G, Girardot R, Perez J (eds.) (2016) *Foxtrot* 3.3.4
43. Zhang F, Ilavsky J, Long GG, Quintana JPG, Allen AJ, Jemian PR (2010) Glassy carbon as an absolute intensity calibration standard for small-angle scattering. *Metall and Mater Trans A* 41(5):1151–1158. <https://doi.org/10.1007/s11661-009-9950-x>
44. Sztucki M (ed.) (2018) *SAXSutilities—on-line processing and analysis of SAXS data*
45. Mix A, Lamm J-H, Schwabedissen J, Gebel E, Stammer H-G, Mittel NW (2022) Monitoring dynamic pre-crystallization aggregation processes in solution by VT-DOSY-NMR spectroscopy. *Chem Commun (Camb)* 58(21):3465–3468. <https://doi.org/10.1039/d1cc05925d>
46. Hartmann D, Thorwart T, Müller R, Thusek J, Schwabedissen J, Mix A, Lamm J-H, Neumann B, Mittel NW, Greb L (2021) The structure of Bis(catecholato)silanes: phase adaptation by dynamic covalent chemistry of the Si-O bond. *J Am Chem Soc* 143(44):18784–18793. <https://doi.org/10.1021/jacs.1c09746>
47. Lamm JH, Niermeier P, Mix A, Chmiel J, Neumann B, Stammer HG, Mittel NW (2014) Mechanism of host-guest complex formation and identification of intermediates through NMR titration and diffusion NMR spectroscopy. *Angewandte Chemie (International ed. in English)* 53(30), 7938–7942. <https://doi.org/10.1002/anie.201402145>
48. Cohen Y, Avram L, Frish L (2005) Diffusion NMR spectroscopy in supramolecular and combinatorial chemistry: an old parameter–new insights. *Angewandte Chemie (International ed. in English)* 44(4), 520–554. <https://doi.org/10.1002/anie.200300637>
49. Caracciolo G, Pozzi D, Caminiti R, Marchini C, Montani M, Amici A, Amenitsch H (2007) Transfection efficiency boost by designer multicomponent lipoplexes. *Biochem Biophys Acta* 1768(9):2280–2292. <https://doi.org/10.1016/j.bbame.2007.06.027>
50. Dargel C, Gräbitz-Bräuer F, Geisler R, Fandrich P, Hannappel Y, Porcar L, Hellweg T (2021) Stable DOPG/glycyrrhizin vesicles with a wide range of mixing ratios: structure and stability as seen by scattering experiments and cryo-TEM. *Molecules (Basel, Switzerland)* 26(16):4959. <https://doi.org/10.3390/molecules26164959>
51. Sreij R, Prévost S, Dargel C, Dattani R, Hertle Y, Wrede O, Hellweg T (2018) Interaction of the saponin aescin with ibuprofen in DMPC model membranes. *Mol Pharm* 15(10):4446–4461. <https://doi.org/10.1021/acs.molpharmaceut.8b00421>
52. Glatter O, Strey R, Schubert KV, Kaler EW (1996) III. Experimental techniques: small angle scattering applied to microemulsions. *Berichte der Bunsengesellschaft für physikalische Chemie* 100(3), 323–335. <https://doi.org/10.1002/bbpc.19961000319>
53. Strey R, Glatter O, Schubert K-V, Kaler EW (1996) Small-angle neutron scattering of D 2 O-C 12 E 5 mixtures and microemulsions with n -octane: direct analysis by Fourier transformation. *J Chem Phys* 105(3):1175–1188. <https://doi.org/10.1063/1.471960>
54. Iampietro DJ, Brasher LL, Kaler EW, Stradner A, Glatter O (1998) Direct analysis of SANS and SAXS measurements of catanionic surfactant mixtures by Fourier transformation. *J Phys Chem B* 102(17):3105–3113. <https://doi.org/10.1021/jp973326b>
55. Huang J-B, Zhao G-X (1995) Formation and coexistence of the micelles and vesicles in mixed solution of cationic and anionic surfactant. *Colloid Polym Sci* 273(2):156–164. <https://doi.org/10.1007/BF00654013>
56. Opatowski E, Lichtenberg D, Kozlov MM (1997) The heat of transfer of lipid and surfactant from vesicles into micelles in mixtures of phospholipid and surfactant. *Biophys J* 73(3):1458–1467. [https://doi.org/10.1016/S0006-3495\(97\)78178-5](https://doi.org/10.1016/S0006-3495(97)78178-5)
57. Vignoli Muniz GS, Souza MC, Duarte EL, Lamy MT (2021) Comparing the interaction of the antibiotic levofloxacin with zwitterionic and anionic membranes: calorimetry, fluorescence, and spin label studies. *BBA-Biomembranes* 1863(7):183622. <https://doi.org/10.1016/j.bbame.2021.183622>

Publisher's Note Springer Nature remains neutral with regard to jurisdictional claims in published maps and institutional affiliations.